A ternary PEDOT-TiO2-reduced graphene oxide nanocomposite for supercapacitor applications

Article (Accepted Version)

A Ternary PEDOT-TiO_2-Reduced Graphene Oxide Nanocomposite for Supercapacitor Applications

Deniz GULERCAN[1], Daniel Commandeur[2], Qiao Chen[2], Abdulkadir Sezai SARAC[1*]

[1] Department of Chemistry & Polymer Science and Technology, Istanbul Technical University, 34469 Maslak, Istanbul, Turkey

[2] Department of Chemistry, School of Life Sciences, University of Sussex, Brighton BN1 9QJ, United Kingdom

*Corresponding Author: sarac@itu.edu.tr

Running Heads: Capacitive behavior of PEDOT-TiO_2-rGO Nanocomposites

Abstract: A ternary composite of PEDOT was prepared with TiO_2 via emulsion polymerization method adjusting various weight ratios of TiO_2 to PEDOT and synthesized rGO was then blended with this composite. The FTIR, UV–Vis and XRD analysis displayed characteristic features of PEDOT and TiO_2. The morphology of the nano-hybrid structure was additionally investigated by SEM analysis. Pore size and surface area analysis of particles were characterized by BET method. The electrochemical analysis showed that the specific capacitance (C_{sp}) for PEDOT-TiO_2-15-rGO was 18.9 $F.cm^{-2}$ at 0.1 mA g^{-1} current density.

***Keywords**:* PEDOT, TiO_2, electrochemistry, emulsion polymerization, spectroscopy.

Introduction

Over last decades nano-hybrid structures of conductive polymers and inorganic materials have been the interest of much research. Nanostructured TiO_2 has many advantages over other metal oxides for incorporation into such hybrids, for example low-toxicity, high stability and low

cost. It has therefore been used for a wide range of applications like photoelectrochemical water splitting, sensors, supercapacitors and photovoltaic cells.[1-4] Among conductive polymers PEDOT (poly3,4-ethylenedioxythiophene), is one of the most frequently used polythiophene derivatives due to its low band gap, good stability and low oxidation potential.[5] On the other hand, PEDOT has a tendency to aggregate which results in less active surface area for charge transfer.[6] In order to overcome this problem, metal oxides and graphene materials have been incorporated into PEDOT. PEDOT and TiO_2 composites have been studied for photoelectrochemical cells,[7,8] OLEDs,[9] solar cells, [10-12] supercapacitors[13] and sensors.[14-16] Furthermore, it has been shown that graphene oxide (GO) and reduced graphene oxide (rGO) enhance polymers' performance in various studies.[17-23] A significant number of studies about PEDOT-graphene nanocomposites have been carried out to investigate their capacitive behavior.[24-27] Although TiO_2 has poor conductivity, compared to graphene and its derivatives, it provides a synergistic improvement to capacitance when combined with PEDOT.[28] This synergistic effect is based on interaction between hydrophilic Ti-O groups in TiO_2 and sulfur elements in PEDOT. Very recently, Tong *et al*. developed an improved method to fabricate a vapor phase polymerization, PEDOT-TiO_2 composite fiber and they obtained the highest specific capacitance of composite fibers to date, 87.9 F g^{-1} at a temperature of 50°C.[29] Patil *et al*. developed a ternary nanocomposite with PEDOT:poly(styrene sulfonate), MnO_2 nanowires and graphene oxide (PMn-GO),[30] which achieved a specific capacitance of 841 Fg^{-1} at a scan rate of 10 mVs^{-1}. Wang *et al*. prepared another ternary electrode material, based on graphene, tin oxide (SnO_2) and PEDOT with a maximum specific capacitance of 180 $F.g^{-1}$ in 1 M Na_2SO_4 aqueous electrolyte.[31]

Herein, new PEDOT-TiO_2-reduced-graphene oxide based ternary nanocomposite was developed for use as a supercapacitor electrode, achieving a capacitance of 18.9 $F.cm^{-2}$, presenting a 92% enhancement over PEDOT-rGO at a 0.1 mA g^{-1} current density. Figure 1 shows a schematic representation of the synthesis of the PEDOT-TiO_2- rGO nanocomposite electrode.

Experimental

Materials. 3, 4-Ethylenedioxythiophene (EDOT; 95% pure) was used as the monomer and sodium dodecylsulfate (SDS) as the surfactant, both purchased from Fisher Scientific. P25 TiO_2 nanoparticles (particle size <100 nm) were purchased from Evonik industries AG. Graphene oxide (GO) was purchased from Grafen Chemical industries, Turkey. The oxidant, ammonium peroxydisulfate (APS; AR grade), was purchased from Acros organics (98% pure). Anhydrous Sodium Sulfate (Na_2SO_4), Hydroiodic acid (HI), ethanol, methanol, isopropanol,[30] acetone and dimethylformamide (DMF) were purchased from VWR chemicals. Deionized water was used as the solvent.

Fluorine-doped tin oxide (FTO) substrates (7 Ω $sq.^{-1}$, Sigma Aldrich) were used as the base for working electrodes. They were cleaned by sonicating in acetone, isopropanol, and ethanol sequentially, cleaned FTO substrates were dried in oven at 100°C for 24h.

Synthesis of PEDOT and PEDOT-TiO_2 Nanoparticles. TiO_2 (P25) nanoparticles (0.034 g) were dispersed in 45 mL of distilled water using ultrasonic vibration (Ultrasonic Homogenizer sonicator cell distruptor 300 W) at room temperature for 20 min. Sodium dodecyl sulfate (0.23 g) was added to TiO_2 dispersion and magnetically stirred for 30 min.[32] 0.25 mL (2.4 mmol) EDOT monomer was added drop wise to the dispersion, and followed by stirring for 1 h, before

adding APS.[33-35] The molar ratio of monomer (EDOT) to oxidant was taken to be 1:2.5. Particles were centrifuged at 3000 rpm and subsequently washed with ethanol and methanol.[36,37] The pure polymer PEDOT was synthesized with the same method as that of the PEDOT-TiO_2 composite. The particles were dried in the oven at 100°C for 24h. The EDOT concentration was kept constant for the preparation of PEDOT-TiO_2 nanoparticle composites. However, the TiO_2 nanoparticle weight percentage (wt %) was varied to 5%, 10%, 15% and 20% and labelled as PEDOT-TiO_2-5, PEDOT-TiO_2-10, and PEDOT-TiO_2-15, PEDOT-TiO_2-20 respectively.[37,38]

Figure 1.

Preparation of PEDOT-TiO_2-rGO composites. Reduced graphene oxide was prepared by using the highly-effective, hydrohalic acid reduction method to convert, graphene oxide (GO) flakes into highly conductive reduced graphene oxide particles.[39] The ternary PEDOT-TiO_2-rGO composites were prepared by mixing PEDOT-TiO_2 composites with rGO. Briefly, rGO and PEDOT-TiO_2 particles were dispersed in DMF separately and the dispersions were ultrasonicated at room temperature for 20 min to obtain homogeneous dispersions. The separate dispersions were then mixed and ultrasonicated together. The weight ratio between rGO and PEDOT-TiO_2 was taken 1:1 for the all PEDOT-TiO_2-rGO samples.

Structural Characterization. Ultraviolet–visible (UV–vis) measurements were carried out on (Perkin-Elmer, PDA Lambda 265) spectrometer in the wavelength range 200–1000 nm.

The purified composites were analyzed by ATR-FTIR (Perkin-Elmer-Spectrum One) to investigate the bonding properties in the wavelength range 400–4000 cm^{-1}. The crystallographic nature of the as-prepared composites was examined using powder X-ray diffractometer (XRD, Siemens

D500) with nickel-filtered Cu-Kα target (λ = 1.5406 Å) at a scan rate of 0.02°/s. Scanning electron microscopy (SEM) (Jeol, JSM-820) was used to analysis of the microstructure and morphology of the synthesized composites using an accelerating voltage of 30 kV and vacuum pressure of 10^{-8}–10^{-10} mm Hg. Surface area and pore size of the samples were measured by Brunauer–Emmett–Teller method (BET), (Beijing, JWGB Sci&Tech, Co. Ltd.) to further investigate the structures. The samples were pre-treated by heating to 100°C under dynamic vacuum (5×10^{-4} Pa) for 2 hours. Nitrogen adsorption isotherms were recorded at liquid nitrogen temperature (−180°C) for a relative pressure (P/P_0) range between 0 and 1. The specific surface area was calculated using the Brunauer–Emmett–Teller (BET) equation for relative pressures between 0.05 and 0.15. The Barrett-Joyner-Halenda (BJH) method was used for the pore size analysis and the density function theory (DFT) model for calculating the pore size distribution from adsorption isotherms.

Results and Discussion

UV-Vis Spectrophotometric Studies. In order to analyze the formation of PEDOT, PEDOT-TiO_2 and the structure of TiO_2 nanostructures by UV-Vis spectroscopy, samples were dispersed in ethanol and concentration of 4 mg/mL. Figure 2 shows the UV-Vis spectra of synthesized pure PEDOT and PEDOT-TiO_2 nanocomposites, inset spectrum shows the absorption behavior of pure TiO_2. The shoulder around 320 nm can be seen in UV-Vis absorption spectrum of pure TiO_2 in ethanol,[40] PEDOT has absorption bands at around 336 and 794 nm.[13] The bipolaron absorption band of PEDOT at 794 nm is ascribed to the π-π* transition and a high level of doping.[41] The

observed blue shifting of the 336 nm absorption band can be attributed to incorporation of TiO_2 supporting the interaction between PEDOT and TiO_2.[13,32]

Figure 2.

ATR-FTIR Studies. The structures of nanocomposites obtained using various weight ratios were investigated using ATR- FTIR spectroscopy. Figure 3 displays ATR-FTIR spectra for pure PEDOT and PEDOT-TiO_2 composites in the region 400-4000 cm^{-1}.

Figure 3.

The main characteristic bands of PEDOT at 1523 and 1400 cm^{-1} are assigned to the C-C and C=C stretching of the quinoidal structure in the thiophene ring and thiophene ring, respectively. The peaks at 1173, 1131 and 1026 cm^{-1} correspond to the C-O-C stretching vibration of the ethylenedioxy group. Further FTIR bands from the C–S vibrations in the thiophene ring can be seen at 965, 823, and 683 cm^{-1}.[42,43] Although there are not many differences in the FTIR spectra of PEDOT–TiO_2 composites for various weight ratios, the peaks at 1523, 1400, 1173, 1131 and 1026 cm^{-1} are shifted to 1477,1353, 1137 and 1063 cm^{-1} respectively for PEDOT–TiO_2 composites (Figure 3.) appearing more sharp than pure PEDOT. [38] A minor peak for Ti-O-Ti at 457 cm^{-1} was hardly observed in FTIR spectrums for PEDOT-TiO_2 composites. The wavelength peak shifts of about ~ 37-47 nm can be attributed that interactions of EDOT monomer with TiO_2 during polymerization in the presence of SDS surfactant.[32]

XRD studies. The crystal structure of prepared nanoparticles were observed using powder XRD. Figure 4 displays XRD pattern for TiO_2, PEDOT and PEDOT- TiO_2 nanoparticles. PEDOT exhibits a

broad peak at around 25° and a small sharp peak at 20.50° indicating a small degree of crystallinity.[44] The XRD pattern of TiO_2 display characteristic 2θ values, the peak assignments to (hkl) planes were as follows: 25.02 (101), 27.12 (110), 35.86 (103), 37.46 (004), 38.4(112), 47.80 (200), 53.82 (105), 54.74 (211), 62.40 (204) and 68.60 (116), respectively. These peaks represent d-spacing characteristic of heterocrystalline anatase (JCPDS No.73-1764).[45]

Figure 4.

The XRD patterns of PEDOT-TiO_2 composites with different weight ratios are displayed in Figure 4, exhibiting peaks at 25.08°, 27.0°, 37,60°, 47.80°,53.70°, 54.80°, 62.30° and 68.40°. As the TiO_2 amount increases in the hybrid structures, the intensity of the assigned peaks increases, while the peaks show small shifts towards lower diffraction angle.[46,47] The XRD results confirms that the incorporation of TiO_2 nanoparticles successfully modified the π-π* interchain stacking of PEDOT chains in the hybrid nanocomposites. This caused them to become more ordered, leading to a reduction in distance of interchain hopping [48,49] further confirmed by EIS results.

Morphology and Surface Area Characterization. The morphology of the samples was characterized by scanning electrode microscopy. SEM images can be seen in Figure 5 (a-f). The pure material components of the composite can be found in Figure 5 (a-c), displaying distinctive morphologies that can be identified in the ternary composites in Figure 5 (d-f). The images confirm the spectral characterization of nanostructures as it exhibits clearly the change of the PEDOT spherical grain shape in Figure 5 (a) to a sponge-like structure with the incorporation of 10 wt% TiO_2 nanoparticles in Figure 5 (d). In this sample the rough surface confirms the porosity

of the material, although this composite does most closely resemble the PEDOT due to effective embedding of the TiO_2 in the bulk.

For the PEDOT-TiO_2-15-rGO sample an anomalously large rGO sheet was the focus, confirming the presence of this component in the films, closely resembling pure rGO imaged in Figure 5(c). The effect of TiO_2 weight is clearly significant, acting to break up the continuous PEDOT sheets visible in Figure 5(a), leading to rGO decorated with PEDOT-TiO_2 nanoparticles across its surface. The further addition of TiO_2 is observed in the PEDOT-TiO_2-20-rGO sample, Figure 5(f), where the segregation of PEDOT and TiO_2 is visible. Overall this sample shows the least homogenous composite due to excess quantities of the metal oxide sitting on the surface. This is reflected in a noticeable drop in the mechanical strength of the film at 20 wt% TiO_2, observed as electrochemical measurements were taken.

Figure 5.

It has been shown that the surface area and pore size affect the electrochemical performance of electrode materials.[50] Therefore, pore size and surface area were analyzed using nitrogen adsorption and desorption isotherms (supp.inf). Additionally, the Brunauer–Emmett–Teller (BET) surface area and pore size of the samples have been summarized in Table 1.

A sharp surface area increase can be seen in Table 1, for PEDOT-TiO_2-20 compared with the other compositions. The reason for this is the excess addition of TiO_2 nanoparticles, as the quantity of PEDOT polymer becomes insufficient to encapsulate them.[13] This leads to segregation of the material components and nanoparticles agglomerate on the surface of the

PEDOT-TiO_2 composite. Therefore, PEDOT-TiO_2-20 has the highest surface area, as nanoparticles are no longer embedded in the polymer. The value is an order of magnitude greater than the other composites, greater than, but comparable to pure TiO_2, due to the exposed particles in conjunction with the porous polymer. Furthermore, the agglomorates give a greater proportion of micropores (< 10 nm) which results in monolayer adsorpsion of N_2 gas.

Table 1.

In terms of the shape of isotherms, the PEDOT-TiO_2-15 and PEDOT-TiO_2-10 samples showed similar shape, between types II and IV with a small hysteresis loop. They also display a sudden increase of adsorbed nitrogen volume followed by a plateau at a higher relative pressure (above P/P0 0.6). This indicates the existence of a large number of mesopores (10-50 nm).

The isotherm shape is confirmed by the corresponding pore size range that shows a mesopores percentage of 74.22% and a macropores percentage of 9.27 % for PEDOT-TiO_2-15. Whereas, the percentage of mesopores is 71.12% and 9.53% for macropores in the PEDOT-TiO_2-10 sample. Keeping such a mesoporous structure can provide low-resistance routes for the ions through the porous structure, and therefore, shorter diffusion pathways. Moreover, this structure can increase electrolyte penetration to the deep interfacial regions which may improve charge transport and ion mobility. It can also facilitate the interaction of electrolyte with the active material of the electrode, creating more convenient pathways for electrolyte ion transportation. This provides more electroactive sites for fast energy storage at high current densities. These properties are significant for supercapacitor electrode materials with a large specific capacitance and high-rate charge–discharge ability.[51]

The BET result of PEDOT-TiO_2-20 shows that it has larger surface area. Nevertheless, PEDOT-TiO_2-20 has nearly Type I N_2 isotherm, reveals its microporous structure which blocks further adsorption of N_2 gas. This also confirmed by results of pore size range (72.54 % for < 10 nm). Moreover, it might help to explain its poor capacitance behavior of this nanocomposite for further impedance studies in this study.

Electrochemical characterization. In order to analyze the electrochemical properties of the synthesized composites, cyclic voltammetry (CV), galvanostatic charge-discharge cycling (GCD), and electrochemical impedance spectroscopic (EIS) measurements were employed using three electrode configuration at room temperature in 1 M Na_2SO_4 aqueous electrolyte. Platinum foil was used as counter electrode and the electrochemical potentials were measured against a saturated Ag/AgCl reference electrode. The working electrodes were prepared by drop casting. The as-prepared PEDOT and PEDOT-TiO_2 nanostructures in DMF solution were mixed homogenously with rGO (1:1 wt%) DMF solution and were drop cast onto FTO. The galvanostatic charge-discharge test was performed at different values of constant current density in the potential range of -0.2 to 0.8 V. The specific capacitance was calculated from the charge-discharge curves using following the equation.

$$Csp = \frac{I}{m \times (\Delta V / \Delta t)} \quad (1)$$

Csp is the specific capacitance ($F.g^{-1}$), *I* is the applied charge-discharge current (A), $\Delta V/\Delta t$ is the gradient of the discharge curve ($V.\ s^{-1}$), and *m* is the mass of the active material coated on the FTO electrode.[21] The active electrode mass was taken 200 mg for each sample. The cyclic

voltammograms (CV) and electrochemical impedance spectroscopy (EIS) measurements were performed using a PalmSens^3 electrochemical sensor. The cyclic voltammograms (CV) were recorded at different scan rates from -0.2 to 0.8 V.

Cyclic voltammetry studies. In order to investigate the contribution of TiO_2 and reduced graphene oxide (rGO) to PEDOT's capacitive behavior, CVs were taken for each composites. The cyclic voltammograms are shown in Figure 6. The CVs reveal that each composites have good capacitive behavior as a significant rise in current density at low potential followed by a clear drop at high voltage is observed. In the case of PEDOT-TiO_2-15 composite, the current response was greatest and the shape of the CV curve was a distorted rectangular, indicating the positive effect of TiO_2 (wt%15) on PEDOT capacitance. Hence, PEDOT-TiO_2-15 composite was selected to investigate for various scan rates between 20-200 mV/s. In Figure 6 (b), the current density maxima for the PEDOT-TiO_2-15 electrode increases with the scan rate and represents fast reaction kinetics. Figure 6(c) shows that rGO enhances capacitance of PEDOT-TiO_2 further still. Among the other composites, the PEDOT-TiO_2-15-rGO is optimal, achieving the highest current response and a similar distorted rectangular shape at the scan rate 60 mV.s^{-1}. This distorted rectangle can be ascribed to uncompensated resistance of active electrode material. As seen in Figure 6(d), the more scan rate increases, so too does the current response at a fixed voltage which confirms the pseudo capacitive behavior of the nanostructures. This is due to the interaction of electrolyte with the coated material on the electrode. At fast scan rates, the electrolyte ions can only interact with the surface of electrode. Conversely, the slow scan rate takes longer times, facilitating the ion interactions deep within almost all the pores of the

coated material on the FTO electrode.[52] Another deduction from CVs, is that addition of 20wt% content of TiO_2 to PEDOT dramatically lower the current response and area of CV curve. This is likely due to the component segregation and weak mechanical stability, previously described.

Figure 6.

The ion diffusion rate is crucial for the performance of supercapacitors, this can be evaluated from the scan rate dependence of the peak current density using the Randles-Sevcik Equation.

$$Ip=(2.69\times10^5)n^{3/2}SD^{1/2}CV^{1/2} \quad (2)$$

According to the Randles–Sevcik equation where *Ip* is the peak current*, n* is the electron number, *A* is the surface area (cm^2), *D* is the diffusion coefficient (cm^2/s) and *C* is the concentration (mol/cm^3). If the peak current (I_p) is directly proportional to the square root of scan rate ($v^{1/2}$), it means the system has diffusion-controlled redox behavior. From Figure 7, where I_p is plotted against $v^{½}$, the gradients of the curves were found to be 0.18 (PEDOT-TiO_2-15-rGO), 0.011 (PEDOT-TiO_2-15) and 0.00141 (PEDOT) respectively. These results evidence the much higher apparent diffusion coefficient of PEDOT-TiO_2-15-rGO in comparison to PEDOT and PEDOT-TiO_2-15. This can be explained by large electro-active area as well as more paths for electrolyte ion diffusion.

Figure 7.

The specific mass capacitances of the composites are plotted as a function of the scan rate in Figure 8. For all samples, at a high scan rate, ion diffusion, electron charge transfer and interaction of ions with the coated material on the electrode are relatively slow, therefore the

specific mass capacitance decreases.[52] The value of specific mass capacitance for each sample was calculated from CV measurements, in a fixed potential window for various scan rates. Figure 8 shows that this value for the PEDOT-TiO_2-15-rGO composite was reduced to 52.6% of the initial value when the scan rate reached 200 mV s^{-1} .

As it has been calculated from the CV voltammograms, the specific capacitance ($F.g^{-1}$) of PEDOT was enhanced by 35.4% due to the contribution of rGO, but a further improvement was obtained (89.6%) for PEDOT-TiO_2 composite by addition of rGO at a scan rate of 60 $mV.s^{-1}$. This results displays that TiO_2, as a metal oxide, improves the PEDOT-rGO composite's specific capacitance.

Figure 8.

All the CVs presented in this work have an asymmetric quality, as in the negative potential window the current is greater than in the positive. This feature has been reported previously with microporous carbon electrodes using an identical Na_2SO_4 aqueous electrolyte. The most likely explanation is the effect of ion migration and sieving. As the materials involved contain micropores (as confirmed by BET) the ionic radius will have an effect on its penetration and adsorption in the pores of the sample. In this case the bivalent sulfate anion has a far greater size and therefore will struggle to adsorb at positive potentials, to the same extent as sodium ions at negative potential. Therefore the current in the negative region will be greater as the full surface of the composite is utilized to store charge. [53,54]

Galvanostatic Charge–Discharge Behavior. Galvanostatic charge-discharge (GCD) curves were studied for pure PEDOT, PEDOT-TiO_2 and PEDOT-TiO_2-rGO nanocomposites with various content of TiO_2, at current densities of 0.01 $mA.g^{-1}$ and 0.1 $mA.g^{-1}$. The GCD curves of the PEDOT-TiO_2-rGO composites are shown in Figure 9. The curves showed linear and symmetrical behavior, along with increased specific capacitance for PEDOT-rGO with the incorporation of TiO_2 up to 20 wt% content. The specific capacitance values were calculated using equation 1. The calculated specific mass capacitances for PEDOT-rGO, PEDOT-TiO_2-5-rGO, PEDOT-TiO_2-10-rGO, PEDOT-TiO_2-15-rGO and PEDOT-TiO_2-20-rGO were found to be 0.54, 4.42, 5.75, 9.49 and 1.32 $F.g^{-1}$ respectively. The corresponding specific area capacitances were calculated to be 1.47, 9.74, 11.5, 18.9 and 2.64 $F.cm^{-2}$ respectively, at the current density of 0.1 $mA.g^{-1}$. The PEDOT-rGO sample has the lowest specific capacitance, displaying a positive trend with increasing TiO_2 content up to 20 wt%, in the composites with an equal quantity of rGO. Although the specific capacitance of PEDOT-TiO_2-20-rGO is the lowest among the PEDOT-TiO_2 composites, it is still higher than the PEDOT-rGO composite.

Figure 9.

Electrochemical impedance spectroscopy. Electrochemical impedance spectroscopy (EIS) was performed to investigate the contribution of TiO_2 as well as rGO to PEDOT nanoparticles. To have a good understanding of the interaction between ions in aqueous solution and electrode surface coated with PEDOT-TiO_2-rGO structure schematic representation is given in Figure 10.

Figure 10.

Nyquist plots for the PEDOT-TiO_2 and PEDOT-TiO_2-rGO in 1 M Na_2SO_4 solution are given in Figure 11. (a)-(b).

The Nyquist plots generally showed incomplete semi-circles in the high frequency region for the samples indicating a constant phase element, Q_{cpe}, in parallel with charge transfer resistance, R_{ct}. This is a typical feature of impedance spectra and is likely due to the double layer capacitance. Additionally, PEDOT-TiO_2-10 and PEDOT-TiO_2-15 nanocomposites tended to display a linear region at a 45° angle to the axes (with equal axes spacing) in the low frequency region. This linear aspect is due to the Warburg resistance element, W, implying frequency dependent ion diffusion through the electrolyte (Figure 11(a)).

The series resistance, R_s, is determined as the first value of intercept of the plot with the real impedance (Z') x axis. The PEDOT-TiO_2-10 and PEDOT-TiO_2-15 samples have small R_s values (20.33, 20.28 Ω respectively) compared with PEDOT (56.61 Ω) and PEDOT-TiO_2-5 (26.02 Ω), further confirming the doping effect measured by UV-Vis, leading to improved charge transport. This suggests that a certain amount of TiO_2 (15 wt%) can act as an electronic dopant during polymerization of PEDOT, reducing the resisitivity of the film. The PEDOT-TiO_2-20 nanocomposite was not stable in the electrolyte and it peeled off from FTO electrode which effected the measurement.

After rGO addition to all compositions of PEDOT-TiO_2 nanocomposites, the Nyquist plots (Figure 11 (b)) exhibit the diameter of semi-circles have decreased in the high frequency region. This is caused by a reduction in R_{ct}, which suggests that the contribution of the rGO was the facilatation of interfacial charge-transfer via the Faradaic process at the interface.[55]

As in the Nyquist plots of PEDOT-TiO_2 nanocomposites, the plots of PEDOT-TiO_2-rGO composites show semicircles in high frequency region accompanied by a clear Warburg feature at low frequency. Nevertheless, PEDOT-TiO_2-15-rGO composite clearly shows the smallest semicircle diameter and more vertical line compared with the other PEDOT-TiO_2-rGO composites and PEDOT-rGO. It clearly suggests, PEDOT-TiO_2-15-rGO has better capacitive performance than the other composites.

In order to describe electrochemical properties of the PEDOT-TiO_2-rGO nanocomposites, the equivalent circuit model was used by using Zsimpwin programme. The parameters of the simulated equivalent circuit models obtained from the Electrochemical Impedance spectra are given in Table 2. The χ^2 (chi-squre) values were around 10^{-4} for chosen model which is a function defined as the sum of the squares of the residuals.[56] The equivalent circuit model, $R_s(Q_{CPE}(R_{ct}W))$, is shown in Figure 11 (c).[57] Table 2 clearly shows that, while TiO_2 content increase from 5 to 15 wt% in PEDOT nanocomposites, Rct values significantly decreases from 7305 to 342.5 Ω respectively. Having a lower Rct value proves easier access (less resistance) of charges to electrode surface. On the other hand, there are some deviations from expected trend of Rs values for the composites, it has been shown before in literature that Rs depends on the nature of electrolyte, distance between the working electrode and reference electrode and temperature of electrolyte. Therefore, this deviations can be caused from experimental conditions. But it can be still seen that Rs value of PEDOT decreases more than half with contribution of TiO_2 and rGO. It can also be deduced that increasing the content of TiO_2 in the

composite together with incorporation of rGO provides a more porous structure improving ion diffusion and lowering resistivity.

Figure 11.

Figure 12 shows the relationship of specific capacitance (Csp) and charge transfer resistance (Rct) with the amount of TiO_2 (wt%). The change of R_{ct} and C_{sp} values with the content of TiO_2 validates the improvement in the capacitive performance of PEDOT-TiO_2-rGO when compared to PEDOT-rGO. It supports the data in literature that PEDOT and TiO_2 has the optimum effect on supercapacitance at 15 wt%. This enhancement has been explained by impact on the porosity, surface area and crystallinity of the structure. The amount of TiO_2 is crucial for composite as the 20 wt% addition of TiO_2 in the composite decreased the stability of the electrode and yielded low specific capacitance. [37]

Figure 12.

Table 2.

Conclusions

In this study, we have successfully fabricated and characterized a ternary PEDOT-TiO_2-rGO composite as supercapacitor electrode. Due to the synergistic effects of PEDOT, TiO_2 and rGO in the composites, capacitive performance improved greatly in comparison to pure PEDOT. PEDOT-TiO_2-15-rGO has produced a specific capacitance of 9.49 $F.g^{-1}$, with an area capacitance of 18.9 $F.cm^{-2}$ in Na_2SO_4. These characterized nanocomposites can be used for further application as a supercapacitor in the future.

Acknowledgments. Corresponding author acknowledge the contribution of the COST Action CA15107 (MultiComp).

References

(1) M. Garcia-Tecedor, S. Z. Karazhanov, G. C. Vasquez, H. Haug, D. Maestre, A. Cremades, M. Taeno, J. Ramirez-Castellanos, J. M. Gonzalez-Calbet, J. Piqueras, C. C. You and E. S. Marstein *Nanotechnology*, ***29***, 035401 (2018).

(2) S. MiarAlipour, D. Friedmann, J. Scott and R. Amal *J. Hazard. Mater.*, ***341***, 404 (2018).

(3) K. Nakata and A. Fujishima *J. Photoc. Photobio. C*, ***13***, 169 (2012).

(4) X. Lu, G. Wang, T. Zhai, M. Yu, J. Gan, Y. Tong and Y. Li *Nano lett.*, ***12***, 1690 (2012).

(5) L. Groenendaal, G. Zotti, P. H. Aubert, S. M. Waybright and J. R. Reynolds *Adv Mater.*, ***15***, 855 (2003).

(6) H. Jingbin, D. Yibo, Z. Jingwen, W. Min, E. D. G. and D. Xue *Small*, ***9***, 98 (2013).

(7) R. Bayon, R. Musembi, A. Belaidi, M. Bär, T. Guminskaya, M.-C. Lux-Steiner and T. Dittrich *Sol. Energy Mater. Sol. Cells*, ***89***, 13 (2005).

(8) E. M. J. Johansson, A. Sandell, H. Siegbahn, H. Rensmo, B. Mahrov, G. Boschloo, E. Figgemeier, A. Hagfeldt, S. K. M. Jönsson and M. Fahlman *Synth. Met.*, ***149***, 157 (2005).

(9) N. Gupta, R. Grover, D. S. Mehta and K. Saxena *Displays*, ***39***, 104 (2015).

(10) W. Maiaugree, S. Lowpa, M. Towannang, P. Rutphonsan, A. Tangtrakarn, S. Pimanpang, P. Maiaugree, N. Ratchapolthavisin, W. Sang-aroon, W. Jarernboon and V. Amornkitbamrung *Sci. Rep.*, ***5a***, 15230 (2015).

(11) S. Yasuteru, K. Takayuki, W. Yuji and Y. Shozo *Chem. Lett.*, ***31***, 1060 (2002).

(12) C. Liu, Z. Su, W. Li, F. Jin, B. Chu, J. Wang, H. Zhao, C. S. Lee, J. Tang and B. Kang *Org. Electron.*, ***33***, 221 (2016).

(13) Y. Liu, D. Sun, S. Askari, J. Patel, M. Macias-Montero, S. Mitra, R. Zhang, W. F. Lin, D. Mariotti and P. Maguire *Sci. Rep.*, ***5***, 15765 (2015).

(14) E. Zampetti, S. Pantalei, A. Bearzotti, C. Bongiorno, F. De Cesare, C. Spinella and A. Macagnano *Procedia Eng.*, ***47***, 937 (2012).

(15) H.-H. Duo, J.-Q. Xu, Y.-L. Liu, Z.-H. Jin, X.-B. Hu and W.-H. Huang *J. Electroanal. Chem.*, ***781***, 371 (2016).

(16) C.-T. Wu, P.-Y. Chen, J.-G. Chen, V. Suryanarayanan and K.-C. Ho *Anal. Chim. Acta*, ***633***, 119 (2009).

(17) H. Zhou, G. Han, D. Fu, Y. Chang, Y. Xiao and H.-J. Zhai *J. Power Sources*, ***272***, 203 (2014).

(18) M. Wang, R. Jamal, Y. Wang, L. Yang, F. Liu and T. Abdiryim *Nanoscale Res. Lett.*, ***10***, 370 (2015).

(19) M. Sekkarapatti Ramasamy, A. Nikolakapoulou, D. Raptis, V. Dracopoulos, G. Paterakis and P. Lianos *Electrochim. Acta*, ***173***, 276 (2015).

(20) J. Dalal, A. Gupta, S. Lather, K. Singh, S. K. Dhawan and A. Ohlan *J. Alloys Compd.*, ***682***, 52 (2016).

(21) J. Wen, Y. Jiang, Y. Yang and S. Li *J. Mater. Sci-Mater. El.*, ***25***, (2014).

(22) T. K. Das and S. Prusty *Polym. Plast. Technol. Eng.*, ***52***, 319 (2013).

(23) H.-C. Tian, J.-Q. Liu, D.-X. Wei, X.-Y. Kang, C. Zhang, J.-C. Du, B. Yang, X. Chen, H.-Y. Zhu, Y.-N. NuLi and C.-S. Yang *Biomaterials*, ***35***, 2120 (2014).

(24) A. Sultan and M. Rafat *Mater. Res. Express*, ***5***, 015507 (2018).

(25) N. Kumar, R. T. Ginting and J.-W. Kang *Electrochim. Acta*, ***270***, 37 (2018).

(26) M. Moussa, G. Shi, H. Wu, Z. Zhao, N. H. Voelcker, D. Losic and J. Ma *Mater. Des.*, ***125***, 1 (2017).

(27) W. Yang, Y. Zhao, X. He, Y. Chen, J. Xu, S. Li, Y. Yang and Y. Jiang *Nanoscale Res. Lett.*, ***10***, 222 (2015).

(28) J. Lu, H. Song, S. Li, L. Wang, L. Han, H. Ling and X. Lu *Thin Solid Films*, ***584***, 353 (2015).

(29) L. Tong, J. Liu, S. M. Boyer, L. A. Sonnenberg, M. T. Fox, D. Ji, J. Feng, W. E. Bernier and W. E. Jones *Electrochim. Acta*, ***224***, 133 (2017).
(30) D. S. Patil, S. A. Pawar, J. C. Shin and H. J. Kim *J. Korean Phys. Soc.*, ***72***, 952 (2018).
(31) W. Wang, W. Lei, T. Yao, X. Xia, W. Huang, Q. Hao and X. Wang ***108***, 118 (2013).
(32) E. Eren, G. Celik, A. Uygun, J. Tabačiarová and M. Omastová *Synth. Met.*, ***162***, 1451 (2012).
(33) S.-G. Oh and S.-S. Im *Curr. Appl. Phys.*, ***2***, 273 (2002).
(34) J. W. Choi, M. G. Han, S. Y. Kim, S. G. Oh and S. S. Im *Synth. Met.*, ***141***, 293 (2004).
(35) W. W. Chiu, J. Travaš-Sejdić, R. P. Cooney and G. A. Bowmaker *Synth. Met.*, ***155***, 80 (2005).
(36) P. Nophawan and S. Anuvat *Polym. Int.*, ***63***, 106 (2014).
(37) K. Luan, S. Yao, Y. Zhang, R. Zhuang, J. Xiang, X. Shen, T. Li, K. Xiao and S. Qin *Electrochimica Acta*, ***252***, 461 (2017).
(38) C. Basavaraja, J. K. Kim and D. S. Huh *Macromol. Res.*, ***23***, 649 (2015).
(39) S. Pei, J. Zhao, J. Du, W. Ren and H.-M. Cheng *Carbon*, ***48***, 4466 (2010).
(40) M. Jakob, H. Levanon and P. V. Kamat *Nano lett.*, ***3***, 353 (2003).
(41) X. Zhang, A. G. MacDiarmid and S. K. Manohar *Chem Commun (Camb)*, 5328 (2005).
(42) V. Hernandez, F. J. Ramirez, T. F. Otero and J. T. L. Navarrete *J. Chem. Phys. Lett. C*, ***100***, 114 (1994).
(43) G. Louarn, J. Kruszka, S. Lefrant, M. Zagorska, I. Kulszewicz-Bayer and A. Proń *Synth. Met.*, ***61***, 233 (1993).
(44) T. Y. Kim, C. M. Park, J. E. Kim and K. S. Suh *Synth. Met.*, ***149***, 169 (2005).
(45) B. S. Shirke, P. V. Korake, P. P. Hankare, S. R. Bamane and K. M. Garadkar *J. Mater. Sci-Mater. El.*, ***22***, 821 (2011).
(46) A. Uygun, O. Turkoglu, S. Sen, E. Ersoy, A. G. Yavuz and G. G. Batir *Curr. Appl. Phys.*, ***9***, 866 (2009).
(47) A. K. Thakur and R. B. Choudhary *Synth. Met.*, ***220***, 25 (2016).
(48) R. Ramakrishnan, S. J. Devaki, A. Aashish, S. Thomas, M. R. Varma and N. Kpp *J. Phys. Chem. Lett. C*, ***120***, 4199 (2016).
(49) R. Jamal, Y. Osman, A. Rahman, A. Ali, Y. Zhang and T. Abdiryim *Materials*, ***7***, 3786 (2014).
(50) C. Merlet, B. Rotenberg, P. A. Madden, P.-L. Taberna, P. Simon, Y. Gogotsi and M. Salanne *Nature Materials*, ***11***, 306 (2012).
(51) D. P. Dubal, S. H. Lee, J. G. Kim, W. B. Kim and C. D. Lokhande *Journal of Materials Chemistry*, ***22***, 3044 (2012).
(52) C. Xiang, M. Li, M. Zhi, A. Manivannan and N. Wu *J. Power Sources*, ***226***, 65 (2013).
(53) M. Vujković, L. Matović, J. Krstić, M. Stojmenović, A. Đukić, B. Babić and S. Mentus *Electrochim. Acta*, ***245***, 796 (2017).
(54) V. Dodevski, M. Stojmenović, M. Vujković, J. Krstić, S. Krstić, D. Bajuk-Bogdanović, B. Kuzmanović, B. Kaluđerović and S. Mentus *Electrochim. Acta*, ***222***, 156 (2016).
(55) L. Xie, Z. Hu, C. Lv, G. Sun, J. Wang, Y. Li, H. He, J. Wang and K. Li *Electrochim. Acta*, ***78***, 205 (2012).
(56) H. Dolas and A. S. Sarac *Synth. Met.*, ***195***, 44 (2014).
(57) M. T. Satici and A. S. Sarac *Int. J.Polym. Mater. Po.*, ***64***, 597 (2015).

Figure Captions

Figure 1. Schematic representation of preperation of PEDOT-TiO_2 particles and PEDOT-TiO_2-rGO electrodes.

Figure 2. UV-vis spectra of (a) PEDOT-TiO_2-15 (b) PEDOT-TiO_2-10 (c) PEDOT-TiO_2-5 and (d) PEDOT composites.

Figure 3. ATR-FTIR spectra for (a) PEDOT-TiO_2-5 (b) PEDOT-TiO_2-10 (c) PEDOT-TiO_2-15 and (d) PEDOT samples.

Figure 4. X Ray diffraction pattern for PEDOT and PEDOT–TiO_2 composites.

Figure 5. SEM images of (a) PEDOT, (b) TiO_2, (c) rGO, (d) PEDOT-TiO_2 -10-rGO, (e) PEDOT-TiO_2-15-rGO and (f) PEDOT-TiO_2-20-rGO nanocomposites.

Figure 6. (a) and (c) Cyclic voltammetry (CV) curves of PEDOT-TiO_2 and PEDOT-TiO_2-rGO composites with various weight content of TiO_2 as the electrode materials, obtained at scan rate of 60 $mV.s^{-1}$. (b) and (d) Cyclic voltammetry curves for PEDOT-TiO_2-15 and PEDOT-TiO_2-15-rGO at various scan rates.

Figure 7. Curves of current density versus the square root of scan rate for PEDOT ,PEDOT-TiO_2 and PEDOT-TiO_2-15-rGO at various scan rates.

Figure 8. Specific mass capacitances of PEDOT-rGO and PEDOT-TiO_2-rGO composites at various scan rates from CV measurements.

Figure 9. (a) Galvanic charge–discharge curves performed by maintaining the current density at 0.1 mA $.g^{-1}$ (b) Galvanostatic charge/discharge curves of PEDOT-TiO_2-15/rGO at 0.1, 1 and 10 mA. g^{-1} in 1M Na_2SO_4.

Figure 10. Schematic presentation of double layer at the electrode–electrolyte interface for prepared system.

Figure 11. Nyquist plots of the PEDOT-TiO_2 and PEDOT-TiO_2-rGO composites indicated with measured and calculated data from the model with 0.1 Hz to 10 kHz (a) PEDOT, PEDOT-TiO_2, PEDOT-TiO_2-5, PEDOT-TiO_2-10, PEDOT-TiO_2-15; (b) PEDOT-rGO, PEDOT-TiO_2-5 -rGO, PEDOT-TiO_2-10 -rGO and PEDOT-TiO_2-15 -rGO ; (c) The equivalent circuit model for PEDOT-TiO_2-rGO composites.

Figure 12. Specific capacitance by area and R_{ct} relation with amount (wt%) of TiO_2 in PEDOT-TiO_2-rGO composites.

Table 1. Surface area and adsorption pore range percentage of PEDOT, TiO_2, PEDOT-TiO_2-10, PEDOT-TiO_2-15 and PEDOT-TiO_2-20.

Sample	Pore range percentage (%)			Surface Area($m^2.g^{-1}$)
	< 10.00 nm	10.00 -50.00nm	>50.00 nm	
PEDOT-TiO_2-10	19.35	71.12	9.53	51.6
PEDOT-TiO_2-15	16.51	74.22	9.27	46.1
PEDOT-TiO_2-20	72.54	20.47	6.99	466.3
PEDOT	71.47	25.59	2.94	7.85
TiO_2	74.58	19.05	6.37	292.8

Table 2. Fitting values for the equivalent circuit elements by simulation of the impedance spectra of PEDOT and PEDOT nanocomposites.

Sample	Rs (Ω)	Q_{CPE} (F)	n_{CPE}	Rct (Ω)	W	χ^2
PEDOT	56.61	$7.30x10^{-5}$	0.8	7305	$1.38\ x10^{-3}$	$1.91x10^{-3}$
PEDOT-TiO_2-5	26.02	$1.08\ x10^{-4}$	0.8	3698	$1.23\ x10^{-3}$	$2.56\ x10^{-3}$
PEDOT-TiO_2-10	20.33	$2.00\ x10^{-4}$	0.8	509.6	$1.82\ x10^{-1}$	$9.71\ x10^{-3}$
PEDOT-TiO_2-15	20.28	$8.14\ x10^{-5}$	0.8	342.5	$1.16\ x10^{-3}$	$1.16\ x10^{-3}$
PEDOT-rGO	26.34	$1.48\ x10^{-4}$	0.749	2674	$0.44\ x10^{-3}$	$6.35X10^{-4}$

PEDOT-TiO_2-5-rGO	19.91	1.85 $x10^{-4}$	0.836	38.6	5.77 $x10^{-3}$	3.76 $X10^{-4}$
PEDOT-TiO_2-10-rGO	26.88	2.03 $x10^{-4}$	0.715	37.2	11.0 $x10^{-3}$	4.86 $X10^{-4}$
PEDOT-TiO_2-15-rGO	26.44	2.59 $x10^{-4}$	1	7.41	12.5 $x10^{-3}$	6.68 $X10^{-4}$

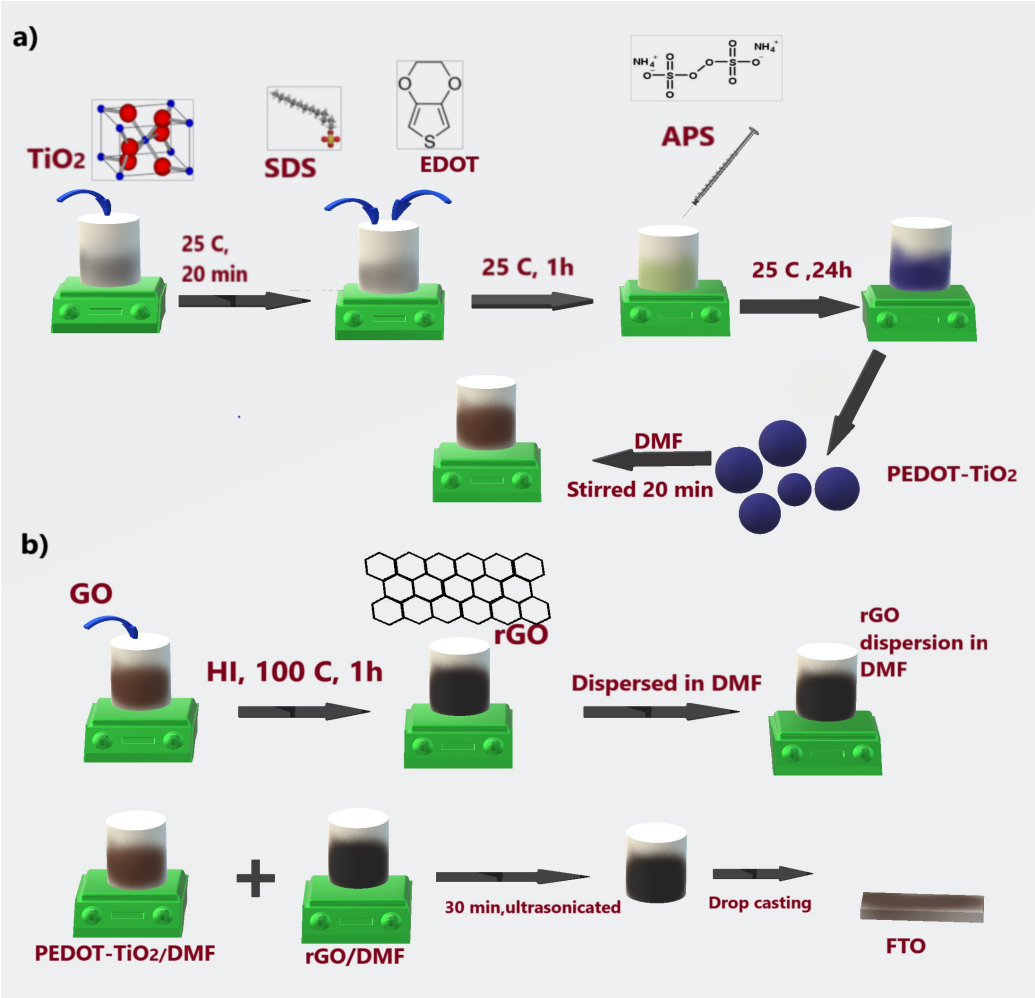

Figure 1. Schematic representation of preparation of PEDOT-TiO_2 particles and PEDOT-TiO_2-rGO electrodes.

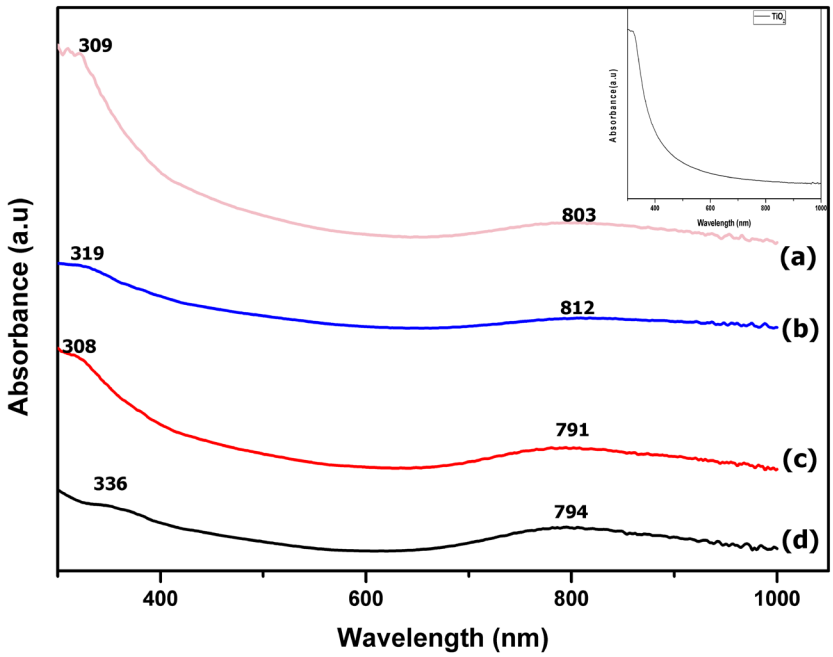

Figure 2. UV-vis spectra of a) PEDOT-TiO2-15 b) PEDOT-TiO2-10 c) PEDOT-TiO2-5 and d) PEDOT composites.

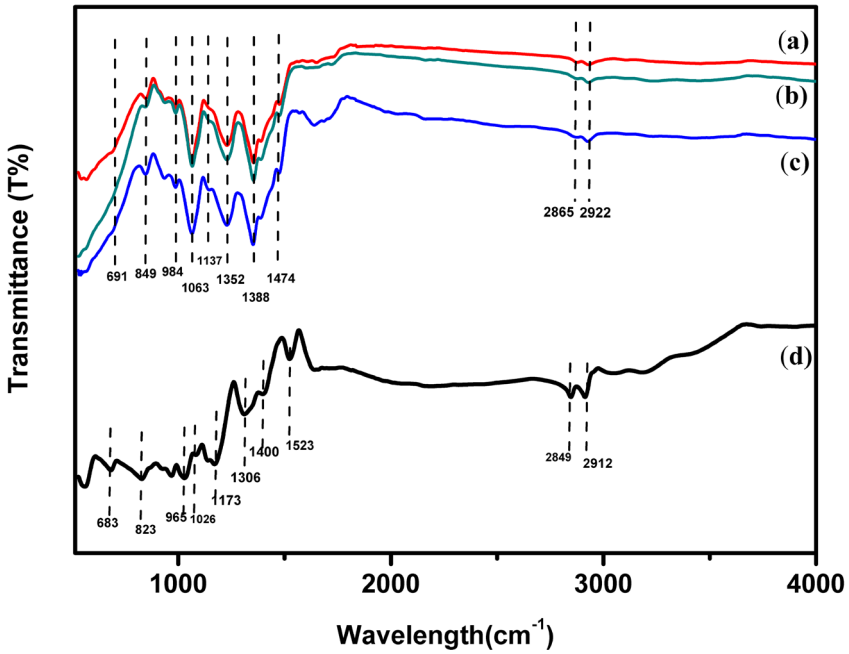

Figure 3. ATR-FTIR spectra for a) PEDOT-TiO_2-5 b) PEDOT-TiO_2-10 c) PEDOT-TiO_2-15 and d) PEDOT samples.

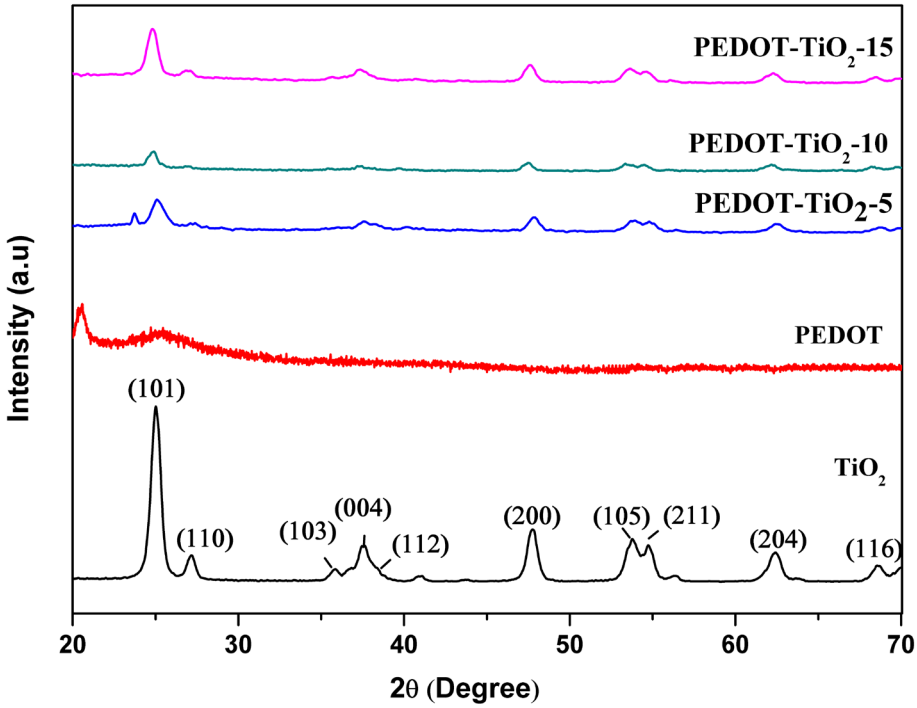

Figure 4. X Ray diffraction pattern for PEDOT and PEDOT–TiO_2 composites.

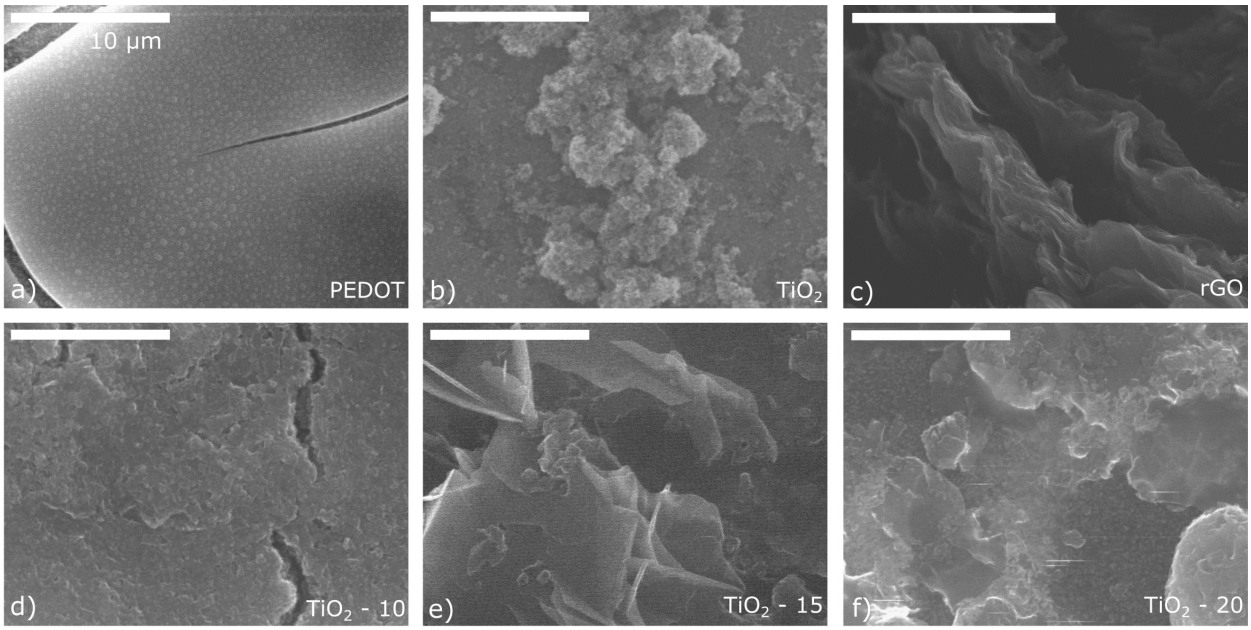

Figure 5. SEM images of a) PEDOT, b) TiO_2, c) rGO, d) PEDOT-TiO_2-10-rGO, e) PEDOT-TiO_2-15-rGO and f) PEDOT-TiO_2-20-rGO nanocomposites.

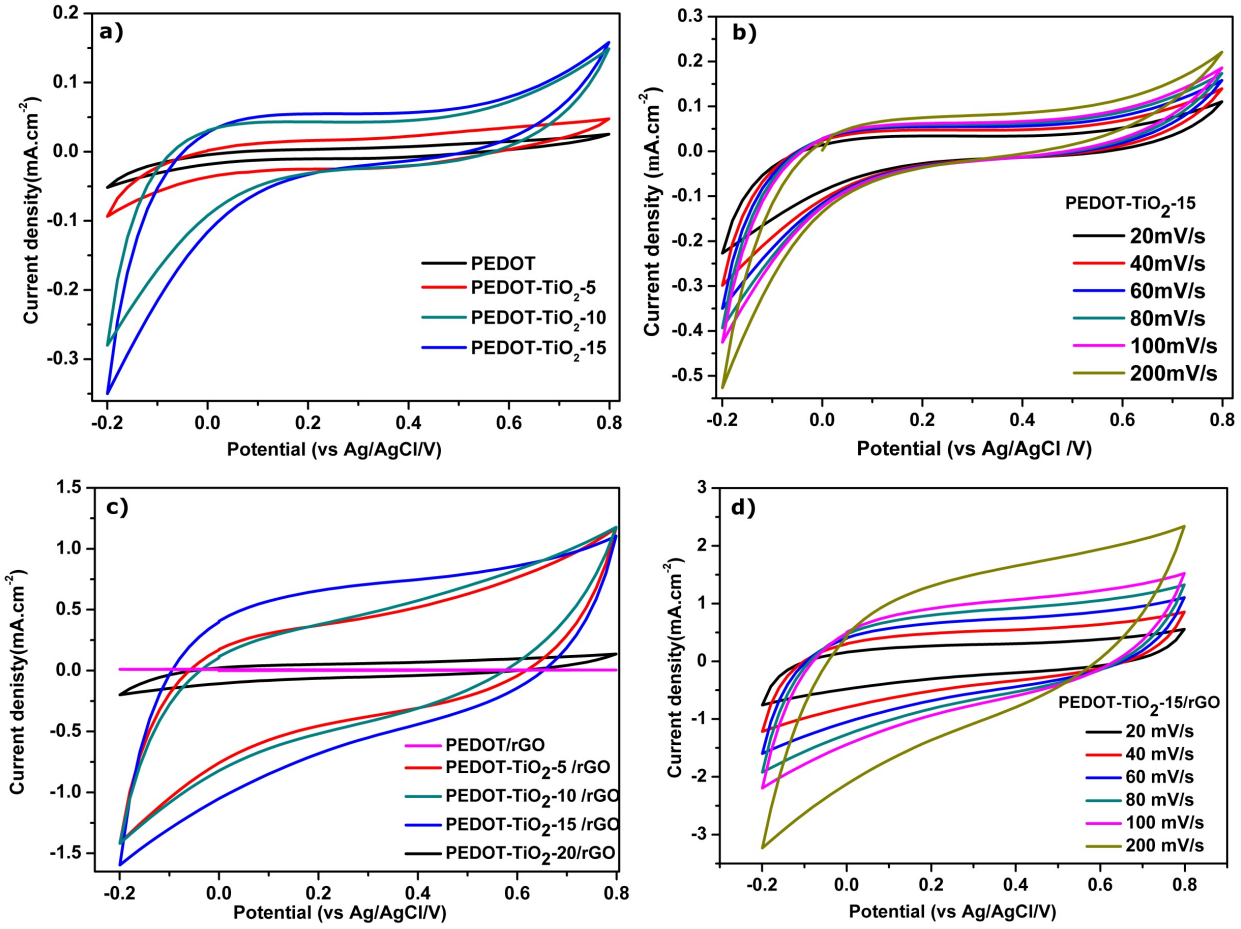

Figure 6. a) and (c) Cyclic voltammetry (CV) curves of PEDOT-TiO_2 and PEDOT-TiO_2-rGO composites with various weight content of TiO_2 as the electrode materials, obtained at scan rate of 60 $mV.s^{-1}$. (b) and (d) Cyclic voltammetry curves for PEDOT-TiO_2-15 and PEDOT-TiO_2-15-rGO at various scan rates.

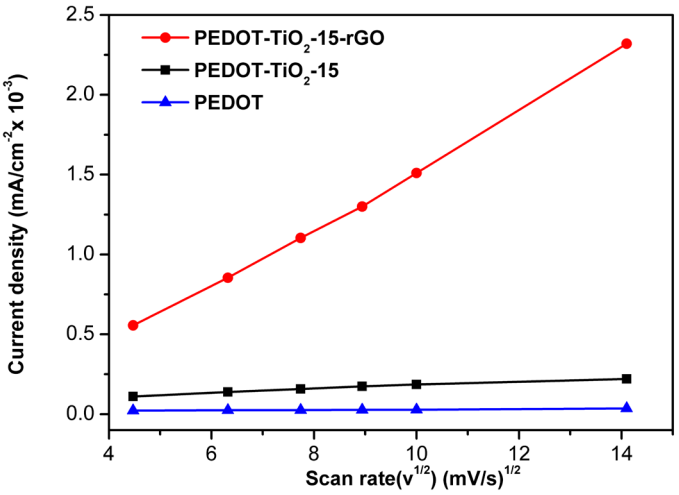

Figure 7. Curves of current density versus the square root of scan rate for PEDOT, PEDOT-TiO_2 and PEDOT-TiO_2-15-rGO at various scan rates.

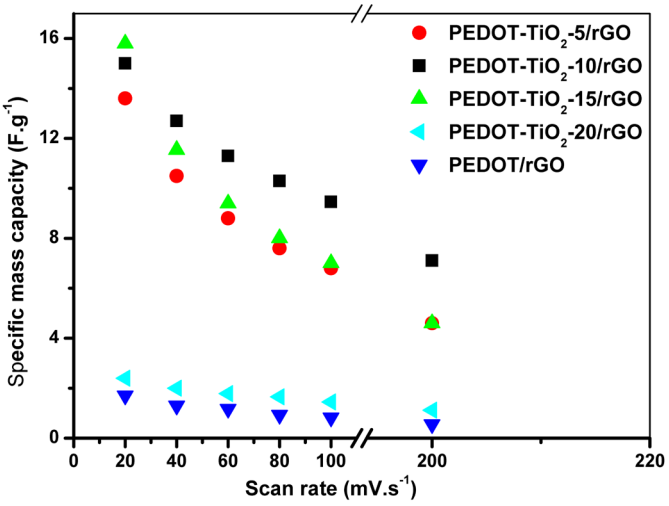

Figure 8. Specific mass capacitances of PEDOT-rGO and PEDOT-TiO_2-rGO composites at various scan rates from CV measurements.

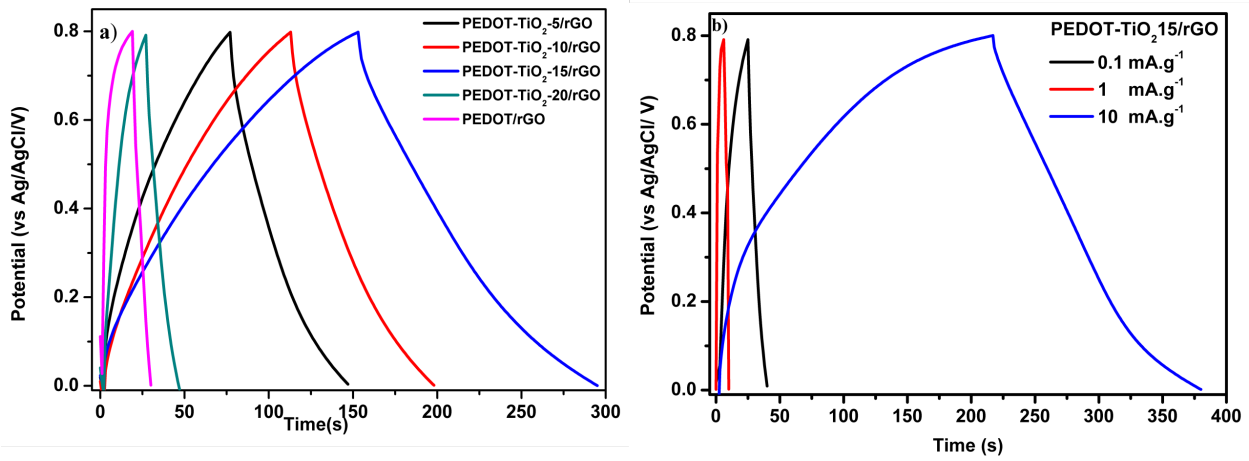

Figure 9. a) Galvanic charge–discharge curves performed by maintaining the current density at 0.1 mA .g^{-1} b) Galvanostatic charge/discharge curves of PEDOT-TiO_2-15/rGO at 0.1, 1 and 10 mA. g^{-1} in 1M Na_2SO_4.

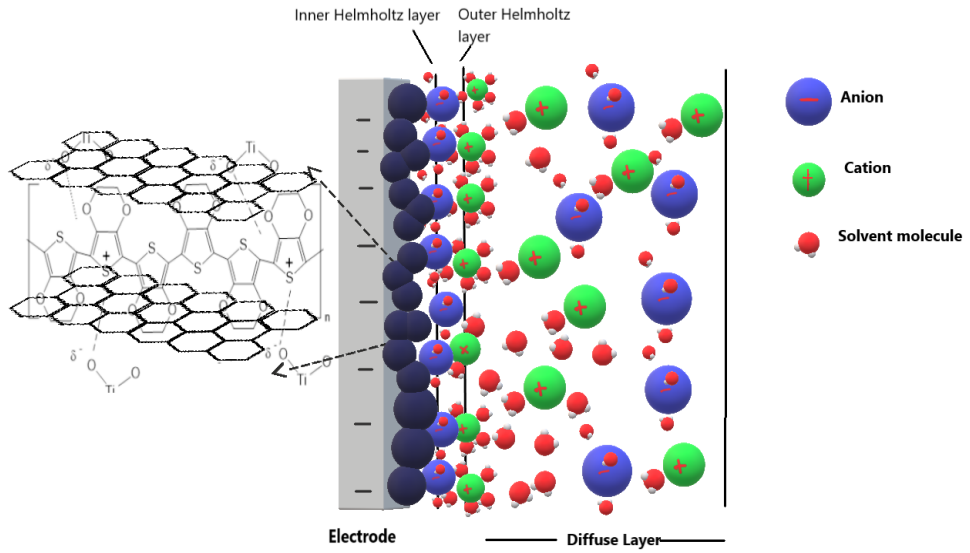

Figure 10. Schematic presentation of double layer at the electrode–electrolyte interface for prepared system.

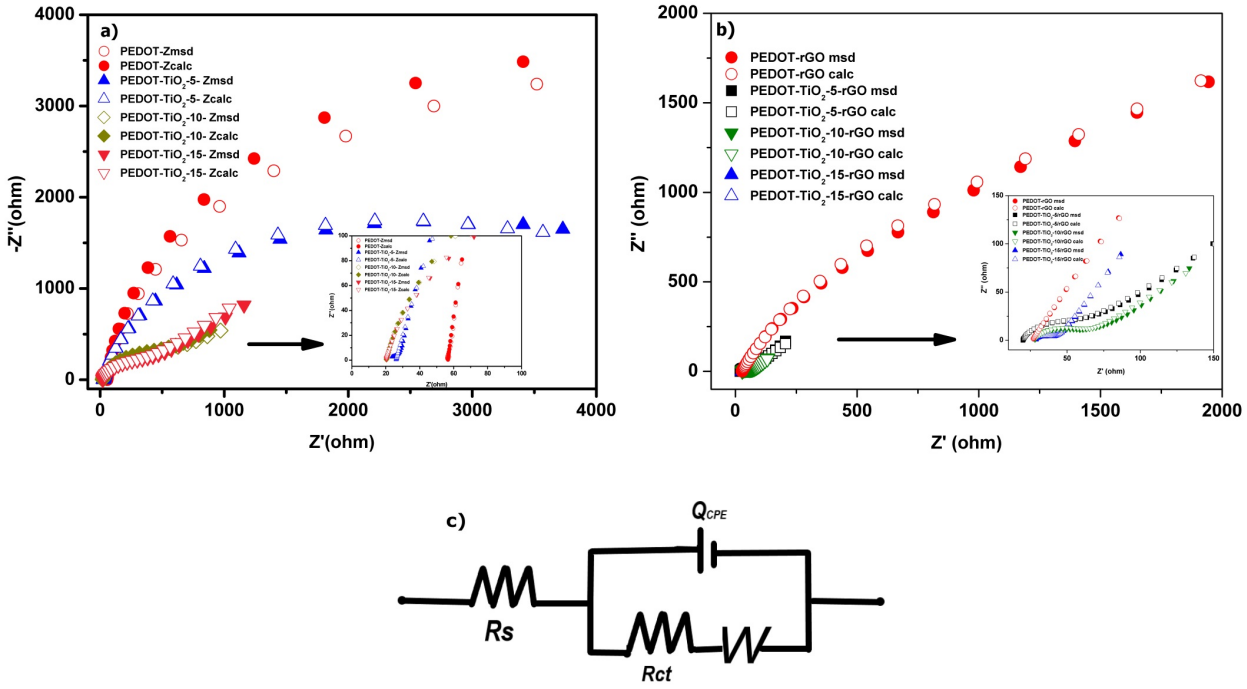

Figure 11. Nyquist plots of the PEDOT-TiO_2 and PEDOT-TiO_2-rGO composites indicated with measured and calculated data from the model with 0.1 Hz to 10 kHz

a) PEDOT, PEDOT-TiO_2, PEDOT-TiO_2-5, PEDOT-TiO_2-10, PEDOT-TiO_2-15;

b) PEDOT-rGO, PEDOT-TiO_2-5 -rGO, PEDOT-TiO_2-10 -rGO and PEDOT-TiO_2-15 -rGO ;

c) The equivalent circuit model for PEDOT-TiO_2-rGO composites.

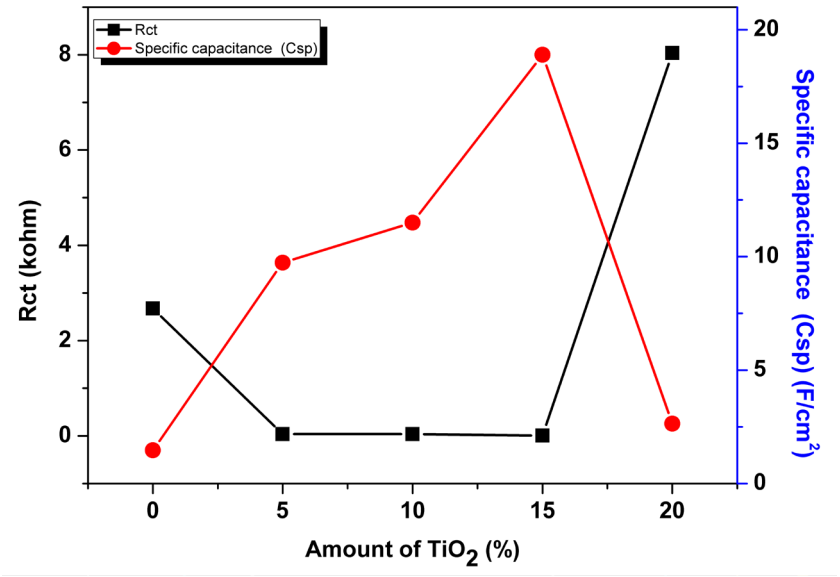

Figure 12. Specific capacitance by area and R_{ct} relation with amount (wt %) of TiO_2 in PEDOT-TiO_2-rGO composites.